Structural Engineering and Mechanics, Vol. 22, No. 2 (2006) 151-167
DOI: http://dx.doi.org/10.12989/sem.2006.22.2.151

Free vibration analysis of rotating cantilever plates using the *p*-version of the finite element method

Sidi Mohammed Hamza-Cherif†

Department of Mechanical Engineering, Faculty of Engineering Sciences, University Abou Bekr Belkaid, 13000, Tlemcen, Algeria

(Received December 24, 2004, Accepted October 21, 2005)

Abstract. A *p*-version of the finite element method in conjunction with the modeling dynamic method using the arc-length stretch deformation is considered to determine the bending natural frequencies of a cantilever flexible plate mounted on the periphery of a rotating hub. The plate Fourier *p*-element is used to set up the linear equations of motion. The transverse displacements are formulated in terms of cubic polynomials functions used generally in FEM plus a variable number of trigonometric shapes functions representing the internals DOF for the plate element. Trigonometric enriched stiffness, mass and centrifugal stiffness matrices are derived using symbolic computation. The convergence properties of the rotating plate Fourier *p*-element proposed and the results are in good agreement with the work of other investigators. From the results of the computation, the influences of rotating speed, aspect ratio, Poisson's ratio and the hub radius on the natural frequencies are investigated.

Key words: Fourier *p*-element; stretch displacement; gyroscopic effect; rotating plates.

1. Introduction

Vibration analysis of rotating cantilever plates is an important subject of study in mechanical engineering. There are many examples in astronautic and aeronautic which can be modelled as rotating cantilever plates, such as solar panels of satellite, turbo-engine blades and helicopter blades. Compared to the plate in the stationary state, the natural frequencies and mode shapes vary significantly with the rotating speed caused by the centrifugal and Coriolis effect. The correct estimation of the natural frequencies at various speeds of rotation is important. Since turbo-engine blades and solar panels are generally idealized as cantilever beams and several papers have been presented in the past for modelling the rotating flexible beams, see for instance Southwell and Gough (1921), Putter and Manor (1967) and Hamza-cherif and Houmat (2004). However this idealization is not correct and gives erroneous results. For rotating plates only a few research works could be found in the literature. Later, Dokainish and Rawtani (1971) used the finite element method to find the natural frequencies and the mode shapes of a cantilever plate mounted on the periphery of a rotating disc. By using the finite element method, Ramamurti and Kielb (1984) give a detailed study to predict the eigenfrequencies of twisted rotating plates, the effects of Coriolis

† Doctor, E-mail: smhamzacherif@caramail.com

acceleration and sweep angle are considered. Recently a new linear dynamic modelling method was introduced by Yoo and Chung (2001) and Yoo and Pierre (2003). This method employs the hybrid deformation variables including a stretch variables and Cartesian variable. The use of the non-Cartesian variables led to capture accurate centrifugal forces caused by the rotation of the plate, and enables one to derive linear equations of motion which include proper motion-induced additional stiffness terms. This modelling method was later successfully utilized to obtain the modal characteristics of rotating beams (see Kane *et al.* 1987, Yoo *et al.* 1995), it is simpler, more consistent, and more rigorous than the conventional methods.

This paper deals with the hierarchical finite element method applied to free vibration analysis of rotating flexible plates. The *p*-version of the finite element method has been limited currently to vibration of plates in the stationary state. The hierarchical concept for finite element shape functions has been investigated during the past 25 years. Babuška *et al.* (1981) established a theoretical basis for *p*-elements, where the mesh keeps unchanged and the polynomial degree of the shape functions is increased; however, in the standard *h*-version of the finite element method the mesh is refined to achieve convergence and the polynomial degree of the shape functions remains unchanged. Since then, standard forms of the hierarchical shape functions have been represented in the literature elsewhere; see for instance (Szabo and Sahrmann 1988, Szabo and Babuška 1991). Meirovitch and Baruh (1983), Zhu (1986) have shown that the hierarchical finite element method yields a better accuracy than the *h*-version for eigenvalues problems. The hierarchical shape functions used by Bardell (1989) are based on integrated Legendre orthogonal polynomials; the symbolic computing is used to calculate the mass and stiffness matrices of beams and plates. Coté and Charron (2001) give the selection of *p*-version shape functions for plate vibration analysis.

In this study a Fourier *p*-version finite element method is applied to the bending free vibration analysis of rotating cantilever plates in conjunction with the method using the arc-length stretch deformation. The transverse displacements are formulated in terms of cubic polynomials functions used generally in FEM plus a variable number of trigonometric shapes functions representing the internals DOF for the plate element, for more details see Houmat (1997, 2001). The natural frequency is investigated for the variation of the rotating speed, dimensions of the plate, Poisson's ratio and hub radius.

2. Kinetic and strain energy expressions

In this section, expressions of strain and kinetic energy of a rotating plate are derived, the plate is considered mounted (cantilevered) on the periphery of a rotating rigid hub of radius R_h, with length a, width b, thickness h and mass per unit area ρ. The Kirchhoff plate assumptions are used in the subsequent analysis (effects of shear deformations and rotary inertia can be neglected).

2.1 Co-ordinates systems

The co-ordinates used to define the geometry of the rotating plate are shown in Fig. 1. Where $\overline{X}, \overline{Y}, \overline{Z}$ denotes the inertial frame and X, Y, Z denotes the moving reference frame attached to the plate and rotating about the X-axis and related to the non-dimensional co-ordinates by

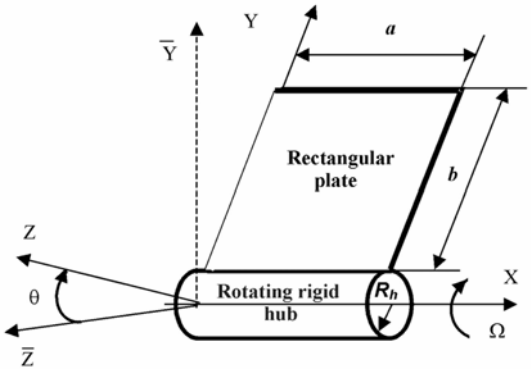

Fig. 1 Configuration of a rotating plate and co-ordinates system

$$\begin{Bmatrix} \zeta \\ \eta \end{Bmatrix} = \begin{bmatrix} \frac{1}{a} & 0 \\ 0 & \frac{1}{b} \end{bmatrix} \begin{Bmatrix} x \\ y \end{Bmatrix} \tag{1}$$

The inertial frame is related to the rectangular moving frame by the orthogonal rotation matrix $[A(\theta)]$, what makes it possible to write

$$R_p = [A(\theta)]r_p \tag{2}$$

where r_p is the position of a material point P in the local X, Y, Z co-ordinate, R_p is the global position vector of a material point P.

The position vector r_p can be written in the following form

$$r_p = (x+u)e_1 + (R_h + y + v)e_2 + we_3 \tag{3}$$

where u, v and w are the components of the elastic deformation in X, Y, Z co-ordinate and θ represents the plate rigid body rotation.

2.2 Kinetic and strain energy expressions

The velocity of the material point P in the inertial frame can be written as

$$\dot{R}_p = [A(\theta)]\dot{r}_p + \Omega[A_\theta(\theta)]r_p \tag{4}$$

where $[A_\theta(\theta)]$ is the derivative $\left[\frac{dA}{d\theta}\right]$ and Ω is the angular speed of the plate.

In the present study, a non-Cartesian variables S and R denoting the arc-length stretch are used instead of the Cartesian distances measure u and v of a point P in the X and Y directions of the

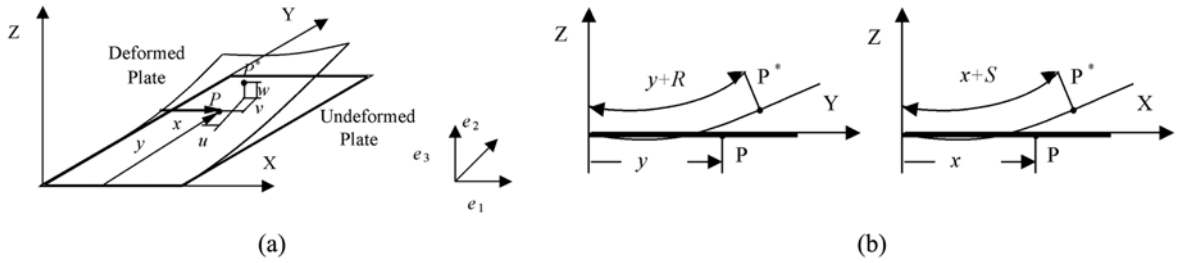

Fig. 2 (a) Deformation variables for a rectangular plate, (b) Non-Cartesian deformation variables

undeformed configuration of the plate respectively, see Fig. 2. Thus a hybrid set (Cartesian variable w with the non-Cartesian variables S and R) is employed to derive the equations of motion.

The geometrical relations between the arc-length stretch S and the Cartesian displacements u, w can be written as

$$S + x = \int_0^x \sqrt{(1 + u_{,\sigma})^2 + (w_{,\sigma})^2}\, d\sigma \tag{5}$$

where $(\,)_{,\sigma}$ replaces $\dfrac{\partial(\,)}{\partial\sigma}$.

Using a binomial expansion of the integrand of Eq. (5)

$$S = u + \frac{1}{2}\int_0^x (w_{,\sigma})^2 d\sigma + \text{H.D.T.} \tag{6}$$

and the time derivative of Eq. (6) is given by the following expression

$$\dot{S} = \dot{u} + \int_0^x w_{,\sigma}\dot{w}_{,\sigma} d\sigma + \text{H.D.T.} \tag{7}$$

In the same way, the geometrical relations between the arc-length stretch R and the Cartesian displacements v, w is given by

$$R + y = \int_0^y \sqrt{(1 + v_{,\sigma})^2 + (w_{,\sigma})^2}\, d\sigma \tag{8}$$

Using a binomial expansion of the integrand of Eq. (8)

$$R = v + \frac{1}{2}\int_0^y (w_{,\sigma})^2 d\sigma + \text{H.D.T.} \tag{9}$$

and the time derivative of Eq. (9) is given by

$$\dot{R} = \dot{v} + \int_0^y w_{,\sigma}\dot{w}_{,\sigma}\, d\sigma + \text{H.D.T.} \tag{10}$$

The kinetic energy of the rotating plate can be found from

$$T = \frac{1}{2}\rho h \int_0^a \int_0^b \dot{R}_p^T \cdot \dot{R}_p dx dy \tag{11}$$

Eq. (11) can be rewritten as

$$T = \frac{1}{2}\rho abh\int_0^1\int_0^1(\alpha^2 + \beta^2 + \dot{u}^2)d\zeta d\eta \tag{12}$$

where

$$\alpha = \dot{R} - \int_0^y(\dot{w}_{,\sigma})(w_{,\sigma})d\sigma + \Omega w \tag{13}$$

$$\beta = \dot{w} - \Omega\left(R_h + y + R - \frac{1}{2}\int_0^y(w_{,\sigma})^2 d\sigma\right) \tag{14}$$

Based on the assumptions given in the beginning of this section, the strain energy is given by

$$U = U_i + U_b \tag{15}$$

The strain bending energy is expressed in non-dimensional co-ordinates as follows

$$U_b = \frac{1}{2}D\frac{b}{a^3}\int_0^1\int_0^1\left[(w_{,\zeta\zeta})^2 + \left(\frac{a}{b}\right)^4(w_{,\eta\eta})^2 + 2\nu\left(\frac{a}{b}\right)^2(w_{,\zeta\zeta})(w_{,\eta\eta}) + 2(1-\nu)\left(\frac{a}{b}\right)^2(w_{,\eta\zeta})^2\right]d\zeta d\eta \tag{16}$$

The exact in-plane strain energy in non-dimensional co-ordinate can be expressed as

$$U_i = \frac{1}{2}abh\int_0^1\int_0^1\left[\frac{E}{1-\nu^2}\left(\frac{1}{a^2}S_{,\zeta}^2 + \frac{1}{b^2}R_{,\eta}^2 + 2\frac{\nu}{ab}S_{,\zeta}R_{,\eta}\right) + G\left(\frac{1}{b^2}S_{,\eta}^2 + \frac{1}{a^2}R_{,\zeta}^2 + \frac{2}{ab}S_{,\eta}R_{,\zeta}\right)\right]d\zeta d\eta \tag{17}$$

3. Plate Fourier *p*-element formulation

In the *p*-version of the FEM, the accuracy of the approximation is improved by increasing the number of shape functions over the element, keeping the mesh constant. The *p*-version of the FEM has, amongst others, the following advantages over the *h*-version:

(i) simples structures can be modeled using just one element, thus there are no inter-element continuity requirements and the assemblage of the elements is avoided;
(ii) the *p*-element in conjunction with the blending functions method can describe the irregular geometry exactly;
(iii) the *p*-version of the FEM gives accurate results with fewer degrees of freedom than the *h*-version, in general monotonic and uniform convergence is guarantied;
(iv) this method offers superior performance in the *h*-version FEM for the vibration analysis of higher frequencies. The refinement in *h*-version is computationally too expansive for capturing high frequency vibrations; it is not well-suited to the vibration analysis of medium or high frequency regimes (Langley and Bardell 1998).

The rotating flexible plate is descritized into one hierarchical finite element, a plate Fourier *p*-element is shown in Fig. 3. The element is fixed at the side ($y = 0$).

The element's nodal DOF are the transverse displacements w, the slopes $w_{,x}$, $w_{,y}$ and $w_{,xy}$ and the stretching displacements S and R at each nodes. The displacement vector formed by the hybrid set

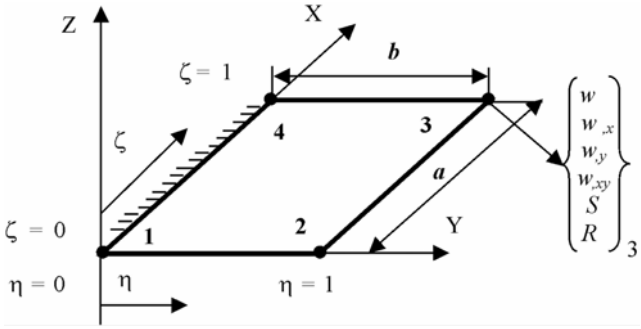

Fig. 3 Plate Fourier *p*-element and nodal displacements

of variables S, R and w is expressed as the combination of the in-plane and out-of plane hierarchical shape functions and can be written as

$$\begin{cases} S(\xi, \eta, t) = \sum_{k=1}^{M_S+2N_S+2} \sum_{l=1} X_{kl}(t) f_k(\xi) f_l(\eta) \\ R(\xi, \eta, t) = \sum_{k=1}^{M_R+2N_R+2} \sum_{l=1} Y_{kl}(t) f_k(\xi) f_l(\eta) \\ w(\xi, \eta, t) = \sum_{k=1}^{M_W+4N_W+4} \sum_{l=1} Z_{kl}(t) g_k(\xi) g_l(\eta) \end{cases} \tag{18}$$

where $f_l(\eta)$ and $g_l(\eta)$ are the shape functions for stretching and bending respectively.

Eq. (18) can be expressed as

$$\begin{Bmatrix} S(\xi, \eta, t) \\ R(\xi, \eta, t) \\ w(\xi, \eta, t) \end{Bmatrix} = [N]\{q\} \tag{19}$$

$[N]$ is the matrix of the shape functions given by

$$[N] = \begin{bmatrix} [N_S] & 0 & 0 \\ 0 & [N_R] & 0 \\ 0 & 0 & [N_w] \end{bmatrix} \tag{20}$$

where

$$[N_S] = [f_1(\xi)f_1(\eta)\ f_1(\xi)f_2(\eta)\ f_1(\xi)f_{N_S+2}(\eta)\ f_2(\xi)f_1(\eta)\ \cdots\ f_{M_S+2}(\xi)f_{N_S+2}(\eta)] \tag{21}$$

$$[N_R] = [f_1(\xi)f_1(\eta)\ f_1(\xi)f_2(\eta)\ f_1(\xi)f_{N_R+2}(\eta)\ f_2(\xi)f_1(\eta)\ \cdots\ f_{M_R+2}(\xi)f_{N_R+2}(\eta)] \tag{22}$$

$$[N_w] = [g_1(\xi)g_1(\eta)\ g_1(\xi)g_2(\eta)\ g_1(\xi)g_{N_W+4}(\eta)\ g_2(\xi)g_1(\eta)\ \cdots\ g_{M_W+4}(\xi)g_{N_W+4}(\eta)] \tag{23}$$

$\{q\}$ is the vector of generalized co-ordinates, expressed as

$$\{q\} = \{X_{11}, X_{12}, \ldots, X_{P_S}, Y_{11}, Y_{12}, \ldots, Y_{P_R}, Z_{11}, Z_{12}, \ldots, Z_{P_w}\}^T \tag{24}$$

Where P_S (=(M_S+2) (N_S+2)), P_R (=(M_R+2) (N_R+2)) and P_w (=(M_w+4) (N_w+4)) are respectively the order of the vector of generalized co-ordinates q^S, q^R and q^w. Where M_S (N_S), M_R (N_R) and M_w (N_w) are the number of trigonometric shape functions in X direction (Y direction).

The group of the shape functions used in this study for bending is given by

$$\begin{cases} g_1(\xi) = 1 - 3\xi^2 + 2\xi^3 \\ g_2(\xi) = \xi - 2\xi^2 + \xi^3 \\ g_3(\xi) = 3\xi^2 - 2\xi^3 \\ g_4(\xi) = -\xi^2 + \xi^3 \end{cases} \tag{25}$$

and the trigonometric shape functions are given by

$$g_{r+4} = \delta_r[-\xi + (2 + (-1)^r)\xi^2 - (1 + (-1)^r)\xi^3] + \sin(\delta_r\xi) \tag{26}$$

The group of the shape functions for stretching is expressed as

$$\begin{cases} f_1(\xi) = 1 - \xi \\ f_2(\xi) = \xi \\ f_{r+2}(\xi) = \sin(\delta_r\xi) \end{cases} \tag{27}$$

$$\delta_r = r\pi, \quad r = 1, 2, 3, \ldots \tag{28}$$

The functions (g_1, g_2, g_3, g_4, f_1, f_2) are those of the FEM (conforming rectangular plate element) necessary to describe the nodal displacements of the element. The trigonometric functions (g_{r+4}, f_{r+2}) contribute only to the internal field of displacement and do not affect nodal displacements (zero displacement and zero slope at each node for bending and zero displacement for stretching). However, products formed between any of the polynomials shape functions and the trigonometric shape functions will constitute what amounts to an edge degree of freedom along the element boundaries. The product involving (g_1, g_3) gives the displacement DOF, whereas, the product involving (g_2, g_4) gives the slope DOF. By consequent, the number of degree of freedom at the interface of the element depends on the number of trigonometric shape functions.

The presented method is restricted to domains, which can be described by one element, only (plate Fourier *p*-element). An extension to more complex situations is possible, where more elements need to be used. Adjacent elements may be joined by ensuring the C^1-continuity of both nodal and edge displacements. For example, equality of displacement and slope at interface of elements along the X direction can be expressed as [$w^i(x,1) = w^{i+1}(x,0)$ and $w^i_{,y}(x,1) = w^{i+1}_{,y}(x,0)$ what gives $Z^i_{m3} = Z^{i+1}_{m1}$ and $Z^i_{m4} = (b^i/b^{i+1})Z^{i+1}_{m2}$]; from where the number of trigonometric shape functions in X direction must be identical for these two elements. Elements with one or more curved edges are mapped by the blending functions method Gordon and Hall (1973), and so the finite

element geometry is exactly the same as the structure geometry. The most attractive particularity of the trigonometric shape functions is that they offer great numerical stability as compared to the polynomial shape functions (numerical instability caused by the computer round-off error in handling high degree polynomials).

The motion is assumed to be harmonic and the expression [Eq. (18)] for S, R, w is inserted into the expressions for the strain energy U and the kinetic energy T, by applying the Euler-Lagrange equations, the linearized system of equations for free vibration of a rotating flexible plate can be obtained.

The system is a two coupled linear equations of motion caused by gyroscopic effect, given by

$$\sum_{m_2=1}^{P_{Rw}} (-\omega^2 M^{Rw}_{m_2,n_2} + 2i\omega\Omega G^{Rw}_{m_2,n_2} + K^{Rw}_{m_2,n_2} + \Omega^2 (R^{Rw}_{m_2,n_2} - M^{Rw}_{m_2,n_2}) + \dot{\Omega} G^{Rw}_{m_2,n_2}) q^{Rw}_{n_2} = 0$$

$$n_2 = 1, 2, 3, \ldots, P_{Rw} \tag{29}$$

and a uncoupled linear equation of motion define the in-plane vibration, is given as follows

$$\sum_{m_1=1}^{P_S} (-\omega^2 M^S_{m_1,n_1} + K^S_{m_1,n_1}) q^S_{n_1} = 0, \quad n_1 = 1, 2, 3, \ldots, P_S \tag{30}$$

Where $M_{m,n}$, $K_{m,n}$ are the coefficients of the conventional trigonometric enriched mass and stiffness matrix, $R_{m,n}$ are the elements of the additional stiffness matrix caused by the centrifuges effect and $G_{m,n}$ are the coefficients of the gyroscopic matrix supposed negligible in this study, the gyroscopic effect takes effect for very high speeds what is not the case in this study, for more details see Ramamurti and Kielb (1984) and Yoo and Chung (2001). In the subsequent analysis the gyroscopic effect is ignored and the angular acceleration $\dot{\Omega}$ is taken as 0, Eq. (29) is reduced to

$$\sum_{m=1}^{P_w} (-\omega^2 M^w_{m,n} + K^w_{m,n} + \Omega^2 (R^w_{m,n} - M^w_{m,n})) q^w_n = 0, \quad n = 1, 2, 3, \ldots, P_w \tag{31}$$

Eq. (31) represents the uncoupled bending equations of motion of a rotating plate.

The different matrices are expressed by the following set of equations

$$R^w_{m,n} = \rho abh \left[\frac{1}{2} (I^{1,1}_{j,l} - A^{1,1}_{j,l}) J^{0,0}_{i,k} + \left(\frac{R_h}{b} \right) (I^{1,1}_{j,l} - B^{1,1}_{j,l}) J^{0,0}_{i,k} \right] \tag{32}$$

and

$$M^w_{m,n} = \rho abh I^{0,0}_{i,k} J^{0,0}_{j,l} \tag{33}$$

$$K^w_{m,n} = \frac{bD}{a^3} \left[I^{2,2}_{i,k} J^{0,0}_{j,l} + \left(\frac{a}{b} \right)^4 I^{0,0}_{i,k} J^{2,2}_{j,l} + 2 \left(\frac{a}{b} \right)^2 (1-\nu) I^{1,1}_{i,k} J^{1,1}_{j,l} + \nu \left(\frac{a}{b} \right)^2 (I^{2,0}_{i,k} J^{0,2}_{j,l} + I^{0,2}_{i,k} J^{2,0}_{j,l}) \right] \tag{34}$$

The coefficients of the matrices $R^w_{m,n}$, $M^w_{m,n}$ and $K^w_{m,n}$ are expressed in terms of the integrals

$$I_{i,k}^{\alpha,\beta} = \int_0^1 g_i^{\alpha}(\xi) \cdot g_k^{\beta}(\xi) d\xi \tag{35}$$

$$J_{j,l}^{\alpha,\beta} = \int_0^1 g_j^{\alpha}(\eta) \cdot g_l^{\beta}(\eta) d\eta \tag{36}$$

$$A_{j,l}^{\alpha,\beta} = \int_0^1 \eta^2 g_j^{\alpha}(\eta) \cdot g_l^{\beta}(\eta) d\eta \tag{37}$$

$$B_{j,l}^{\alpha,\beta} = \int_0^1 \eta g_j^{\alpha}(\eta) \cdot g_l^{\beta}(\eta) d\eta \tag{38}$$

where the indices α and β denote the order of the derivatives.

The exact values of the above integrals can easily be found by using symbolic computation Bardell (1989), which is available through a number of commercial packages.

The indices i, k, j and l represent the numbers of functions used in the assumed displacements field take on the following values

$$i, k = 1, 2, 3, \ldots, M_w + 4 \tag{39}$$

$$j, l = 1, 2, 3, \ldots, N_w + 4 \tag{40}$$

and the indices m, n are expressed in terms of the indices i, k, j and l as

$$m = j + (i - 1)(N_w + 4) \tag{41}$$

$$n = l + (k - 1)(N_w + 4) \tag{42}$$

Table 1 Convergence study of the five lowest frequency parameters ω^* of rotating cantilever plates ($\mu = 10$, $R_h/b = 0$, $\nu = 0.3$)

$M_w(= N_w)$	1st	2nd	3rd	4th	5th
0	5.169	9.781	30.853	43.114	50.120
4	5.042	9.018	26.621	32.284	38.966
5	5.038	9.012	26.603	32.281	38.964
6	5.037	9.010	26.602	32.276	38.952
7	5.036	9.009	26.598	32.275	38.951
8	5.035	9.008	26.598	32.273	38.947
9	5.035	9.007	26.597	32.273	38.946
10	5.034	9.006	26.596	32.272	38.944
11	5.034	9.006	26.596	32.272	38.943
12	5.034	9.006	26.595	32.271	38.942
13	5.034	9.005	26.595	32.271	38.942
14	5.033	9.005	26.594	32.271	38.941
15	5.033	9.005	26.594	32.271	38.940
16	5.033	9.005	26.594	32.271	38.940
Converged solution	5.033	9.005	26.594	32.271	38.940

4. Results and comparison with other work

4.1 Convergence study and comparison

In order to see the manner of convergence, the plate is discretized into one element and the number of trigonometric shape functions is varied.

The frequency parameter ω^* and the angular speed parameter μ are employed in this study.

For a rotating cantilever square plate (μ = 10, R_h/b = 0 and ν = 0.3) as shown in Table 1 as number of trigonometric shape functions is increased from 1 to 16, the relative decreases of the lower frequency parameters ω^* is very small, and highly accurate solutions are obtained despite the use of few hierarchical terms. An uniform and monotonic convergence is guaranteed. The value $M_w = 0$ corresponds to using one 16 DOF rectangular finite element.

In the case of plate in stationary state (μ = 0), the performance of the proposed plate Fourier *p*-element can be verified by comparing the frequency parameters with other references in the case of plate with different boundary conditions. The symbolism S, C and F used in the subsequent analysis denote respectively an edge that is simply supported, clamped and free.

In order to see the manner of convergence of the Fourier *p*-finite element solutions, the number of trigonometric terms is varied (equal terms is used in both directions). For a S-S-S-S square plate ($a = b$ and $\nu = 0.3$), Table 2 clearly shows that rapid convergence from above to the exact values occurs as the number of trigonometric terms is increased from 1 to 4. The results for the ten lowest modes with $M_w = N_w = 4$ are in excellent agreement with exact solutions. The performance of the Fourier *p*-element with that of the polynomial hierarchical finite element Bardell (1992) and that of the 36-degree-of-freedom rectangular finite element on a total degree of freedom basis is also investigated in Table 2. The number of trigonometric terms used in Fourier *p*-element is four and the corresponding number of DOF is 36, the number of polynomials hierarchical terms (formed from the orthogonal legendre polynomials) is six and the corresponding number of DOF is 64, whereas, the number of rectangular finite elements used in both square plate is nine and the corresponding number of DOF is 92. The Fourier *p*-element method gives more accurate solutions with 43% fewer system DOF than the polynomial hierarchical element method solutions and 61% fewer system DOF than the solutions from the rectangular finite element method. Additional applications are to S-F-S-F and C-F-F-F square plates, Tables 3 and 4 show that fast convergence from above to the converged values occurs as the number of trigonometric terms is increased. Tables 3 and 4 also show that the Fourier *p*-element solutions are more accurate than the solutions from the finite element method with fewer systems DOF. All results confirm that the rate of convergence is influenced directly by the trigonometric terms and boundary conditions. It is observed from these tables that the present results are fairly in good agreement with exact solutions and other formulations with fewer DOF used in the computation. This reduction in the number of system DOF leads to large computational savings.

In the case of a cantilever flexible plate mounted on the periphery of a rotating hub, the performance of the proposed plate Fourier *p*-element can be verified by comparing the first five frequency parameters with that of the modal analysis Yoo and Pierre (2003), Southwell method and the finite element method by using ANSYS. The number of trigonometric terms used in Fourier *p*-element is 16 and the corresponding number of DOF is 360. To obtain the finite element solutions (ANSYS), 289 elements (element type used is SHELL 63 with four nodes and stress stiffening capabilities) are employed to divide the plate, the corresponding number of DOF is 1221. Tables 5

Table 2 Convergence and comparison of the ten lowest frequency parameters ω^* for the S-S-S-S square plate ($a = b$, $\nu = 0.3$)

Method		N of DOF	1	2	3	4	5	6	7	8	9	10	% Error 10^{-3}
Present analysis M_w (=N_w)	0	5	20.976	58.992	58.992	92.563	---	---	---	---	---	---	
	1	9	19.739	58.707	58.707	92.563	133.435	133.435	163.281	163.281	226.951	---	
	2	16	19.739	49.348	49.348	78.957	133.435	133.435	158.727	158.727	226.951	248.503	
	3	25	19.739	49.348	49.348	78.957	98.696	98.696	128.305	128.305	177.653	248.503	
	4	36	19.739	49.348	49.348	78.957	98.696	98.696	128.305	128.305	167.783	167.783	
Converged solution	4	36	19.739	49.348	49.348	78.957	98.696	98.696	128.305	128.305	167.783	167.783	0
Polynomial HFEM		64	19.739	49.348	49.348	78.957	98.716	98.716	128.322	128.322	167.987	167.987	20
FEM		92	19.739	49.348	49.348	78.957	98.745	98.745	128.344	128.344	168.085	168.085	50
Exact			19.739	49.348	49.348	78.957	98.696	98.696	128.305	128.305	167.783	167.783	

% Error = (Method-Exact)/Exact

Table 3 Convergence and comparison of the ten lowest frequency parameters ω^* for the S-F-S-F square plate ($a = b$, $\nu = 0.16$)

Method		N of DOF	1	2	3	4	5	6	7	8	9	10	% Error 10^{-3}
Present analysis M_w (=N_w)	0	8	10.906	17.867	43.001	50.134	57.820	86.488	106.512	150.989	---	---	
	1	15	9.809	17.149	38.324	50.092	57.820	81.362	106.232	125.279	132.945	150.989	
	2	24	9.809	17.063	38.324	39.353	48.068	73.808	77.350	115.595	125.279	132.675	
	3	35	9.808	17.063	37.974	39.348	48.068	72.949	77.350	88.631	97.745	115.595	
	4	48	9.808	17.060	37.974	39.348	48.052	72.949	76.455	88.631	97.702	113.777	
	5	63	9.808	17.060	37.956	39.348	48.052	72.894	76.455	88.628	97.702	113.777	
	6	80	9.808	17.060	37.956	39.348	48.050	72.894	76.392	88.628	97.694	113.643	
	7	99	9.808	17.060	37.954	39.348	48.050	72.885	76.392	88.627	97.694	113.643	
Converged solution	7	99	9.808	17.060	37.954	39.348	48.050	72.885	76.392	88.627	97.694	113.643	33
FEM		112	9.808	17.060	37.954	39.348	48.050	72.882	76.378	88.679	97.740	113.611	50
Exact			9.808	17.060	37.953	39.348	48.049	72.881	76.375	88.627	97.691	113.605	

% Error = (Method-Exact)/Exact

Table 4 Convergence and comparison of the ten lowest frequency parameters ω^* for the C-F-F-F square plate ($a = b$, $\nu = 0.3$)

Method		N of DOF	1	2	3	4
Present analysis M_w (=N_w)	0	8	3.518	8.953	28.888	37.415
	1	15	3.487	8.552	21.411	27.483
	3	35	3.476	8.517	21.308	27.219
	5	63	3.473	8.512	21.297	27.203
	7	99	3.472	8.510	21.292	27.200
	9	143	3.472	8.509	21.290	27.200
	11	195	3.471	8.508	21.288	27.199
	12	224	3.471	8.508	21.288	27.199
Polynomial HFEM		360	3.471	8.506	21.284	27.199
FEM						
Ritz			3.454	8.586	21.417	27.437

Method		5	6	7	8	9	10
Present analysis M_w (=N_w)	0	44.245	83.568	96.417	154.430	---	---
	1	31.813	56.923	92.069	115.574	117.284	136.759
	3	31.017	54.326	61.600	64.747	71.519	94.632
	5	30.978	54.230	61.293	64.199	71.043	93.119
	7	30.969	54.206	61.270	64.199	71.001	92.978
	9	30.964	54.198	61.264	64.147	70.987	92.947
	11	30.962	54.194	61.261	64.144	70.980	92.937
	12	30.961	54.193	61.261	64.143	70.978	92.934
Polynomial HFEM		----	----	----	----	----	----
FEM							
Ritz		----	----	----	----	----	----

and 6 show that for a square plate and various values of μ in the case of the hub radius $R_h = 0$ and $R_h = b$ respectively, the results obtained using the present formulation are fairly in good agreement with those of the modal analysis, Southwell method and agree to a remarkable degree for all frequencies parameters.

It is shown in Tables 5 and 6 that the lowest five mode of a rotating square plate obtained by using the Fourier p-element method agree well with those obtained by using ANSYS but with 71% fewer system DOF. This reduction in the number of system DOF leads to large computational savings.

4.2 The effect of varying the angular speed parameters, aspect ratio, Poisson's ratio and hub radius

Individual and joint variation of the angular speed parameters, aspect ratio, Poisson's ratio and

Table 5 Comparison of the first five frequency parameters ω^* for rotating cantilever square plates ($a = b$, $\nu = 0.3$, $M_w = 16$, $R_h = 0$)

μ	Method	1st	2nd	3rd	4th	5th
1	Present method (360)	3.499	8.513	21.404	27.209	31.050
	ANSYS (1221)	3.499	8.519	21.420	27.218	31.097
	Modal analysis	3.515	8.533	21.520	27.353	31.206
	Southwell method	3.513	8.528	21.525	27.402	31.458
2	Present method (360)	3.580	8.531	21.752	27.241	31.322
	ANSYS (1221)	3.580	8.530	21.760	27.251	31.361
	Modal analysis	3.596	8.550	21.865	27.384	31.477
	Southwell method	3.579	8.532	21.894	27.691	32.113
10	Present method (360)	5.033	9.005	26.594	32.271	38.940
	ANSYS (1221)	5.025	8.796	26.316	32.408	38.767
	Modal analysis	5.049	9.032	26.761	32.350	39.078

Table 6 Comparison of the first five frequency parameters ω^* for cantilever plates mounted on the periphery of a rotating hub ($a = b$, $\nu = 0.3$, $M_w = 16$, $R_h/b = 1$)

μ	Method	1st	2nd	3rd	4th	5th
1	Present method (360)	3.717	8.604	21.591	27.250	31.193
	ANSYS (1221)	3.775	8.617	21.649	27.264	31.268
	Modal analysis	3.732	8.624	21.706	27.394	31.350
	Southwell method	3.730	8.614	21.710	27.554	31.760
2	Present method (360)	4.367	8.889	22.468	27.415	31.888
	ANSYS (1221)	4.551	8.914	22.633	27.449	32.035
	Modal analysis	4.380	8.909	22.580	27.557	32.043
	Southwell method	4.376	8.870	22.612	28.288	33.620
10	Present method (360)	13.252	15.275	29.618	43.185	48.691
	ANSYS (1221)	13.952	15.408	29.338	45.908	50.370
	Modal analysis	13.273	15.311	29.792	43.289	48.851

hub radius is found to influence greatly the bending natural frequency.

From the convergence and comparison studies, 16 trigonometric shape functions have been employed in the subsequent analysis, and considered sufficient to insure adequate convergence for the lowest five frequencies.

The natural frequencies are computed for clamped plates mounted on the periphery of a rotating hub, for various values of the angular speed parameter (μ from 0 to 10), the aspect ratio (a/b from 0.25 to 4), the hub radius ($R_h/b = 0$ to $R_h/b = 1$) and the Poisson's ratio (ν from 0 to 0.49). The solid lines in the Figs. 4-6 are for zero hub radius ($R_h = 0$), while the dotted lines are for $R_h/b = 1$.

In this study the coupling effect is supposed negligible, Fig. 4 shows how the frequency of the first five bending modes of a rotating cantilever square plate ($a = b$, $\nu = 0.3$) vary with angular speed parameter. In all cases the bending curves frequency increases with increasing angular speed

parameter. The increasing rates become larger as the hub radius increases. In general for zero hub radius ($R_h = 0$) the form of the modes is preserved through the range of angular speed parameter except for frequency curves 3 and 4 (see Fig. 4). Another interesting phenomenon can be observed in Fig. 4 is called veering modes. When the rotating speed is increased the frequency curves increase and the corresponding mode shapes are changed through centrifugal stiffening, modal interaction can occur between all modes. The third bending frequency curve and the fourth bending curve veer, this indicates that the angular speed produces significant coupling between these two curves. The corresponding modes shapes change with increasing the angular speed parameter and seem to switch their shapes. At veering region ($\mu = 6.68$) the mode shapes become very similar but with opposite concavity of the nodal lines, for more details see Leissa (1974) and Yoo and Pierre (2003).

The frequency variation with aspect ratio (in the range $1/4 \le a/b \le 4$) for a rotating cantilever plate ($\mu = 10$, $\nu = 0.3$) is shown in Fig. 5. The frequencies of the first five modes all increases with increasing aspect ratio a/b, the form of the first, second and third modes is preserved through the range of aspect ratio considered here for $R_h = 0$ and $R_h/b = 1$ respectively. Another interesting phenomenon can be observed in Fig. 5, is called crossing modes, involving the fourth and fifth frequency curves. The crossing region is around $a/b = 1.75$ for $R_h = 0$ and around $a/b = 1.66$ for $R_h/b = 1$. The frequency curves cross when the associated modes of free vibration belong to different symmetry groups, and this in turn leads to a reordering of the modes. The mode reordering that takes place at such a crossover, and an exchange in modal identity is made between mode 4 and 5. At the crossover the mode shapes of the fourth and fifth frequency curves become similar. This feature was first reported by Barton (1951). It is clearly seen from Fig. 5 that after the crossover the fourth mode is preserved through the range of aspect ratio.

Fig. 5 also shows that if the aspect ratio (a/b) increases the dotted lines converge to the solid lines, consequently the hub radius R_h does not have an influence on the frequency parameters.

Fig. 6 gives the trajectory of the lowest frequency parameters for rotating cantilevered square plates ($\mu = 10$ and $a = b$) while varying the Poisson's ratio ν ($0.0 \le \nu \le 0.49$). The conclusion that can be drawn from these curves is that in general the frequency parameters decrease with increasing ν for $R_h = 0$ and $R_h/b = 1$ respectively.

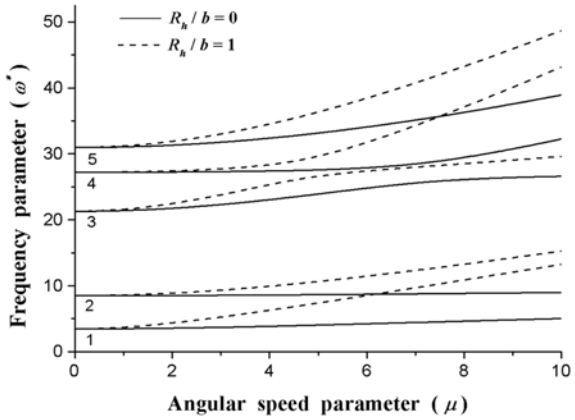

Fig. 4 Frequency parameter variation with the angular speed parameter

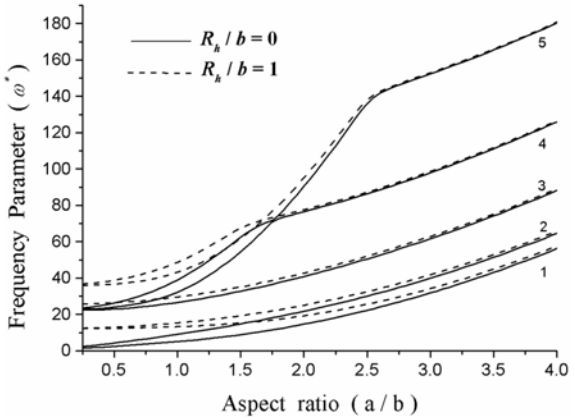

Fig. 5 Frequency parameter variation with aspect ratio (a/b)

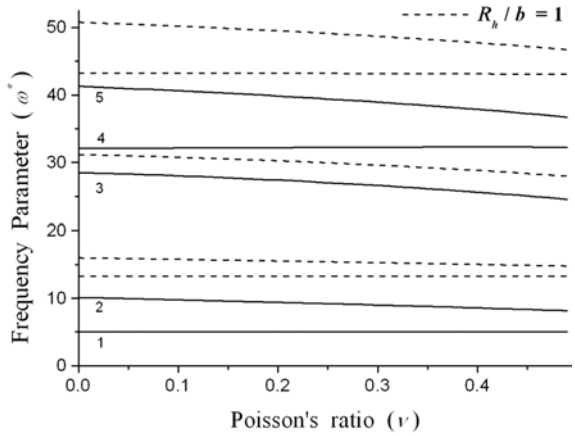

Fig. 6 Frequency parameter variation with Poisson's ratio

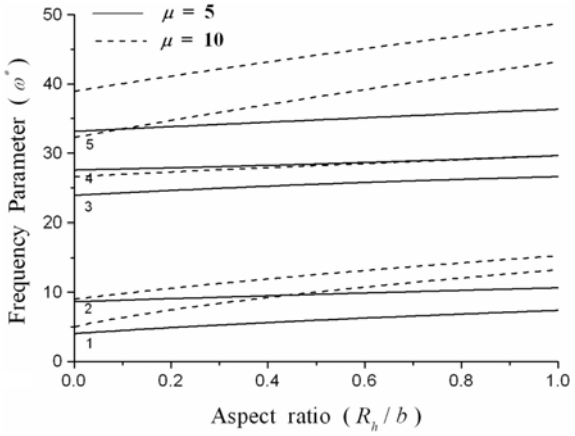

Fig. 7 Frequency parameter variation with aspect ratio (R_h/b)

Fig. 7 gives the trajectory of the lowest frequency parameters for rotating cantilevered square plates while varying the aspect ratio R_h/b ($0 \leq R_h/b \leq 1$) for two angular speed values $\mu = 5$ and $\mu = 10$ ($a = b$ and $\nu = 0.3$). The frequencies of the first five modes all increases with increasing aspect ratio R_h/b. The increasing rates become larger as the angular speed increases.

5. Conclusions

The Fourier *p*-version of the finite element method is developed and used to find the natural frequencies of a cantilever flexible plate mounted on the periphery of a rotating hub in conjunction with the modelling dynamic method using the arc-length stretch deformation. The main conclusions have emerged from this work these are itemized in the following:

(i) Monotonic and uniform convergence is found to occur as the number of trigonometric shape functions is increased.

(ii) For values of angular speed parameter other than zero the convergence is slowed, hence to obtain reliable results, it has been necessary to include a significantly greater number of trigonometric terms than that required in the case of plate in stationary state.

(iii) The dynamic characteristics of rotating cantilever plates are influenced significantly by varying individually or jointly the angular speed parameters μ, the aspect ratio (a/b), the hub radius and Poisson's ratio ν. In general the frequencies parameter increases with increasing μ, (a/b) and (R_h/b) and decreases with increasing ν.

References

Babuška, I., Szabo, B.A. and Katz, I.N. (1981), "The *p*-version of the finite element method", *SIAM Journal on Numerical Analysis*, **18**, 515-545.

Bardell, N.S. (1989), "The application of symbolic computing to hierarchical finite element method", *Int. J.*

Num. Meth. Eng., **28**, 1181-1204.
Bardell, N.S. (1992), "Free vibration analysis of a flat plate using the hierarchical finite element method", *J. Sound Vib.*, **151**, 263-289.
Bardell, N.S. (1992), "The free vibration of skew plates using the hierarchical finite element method", *Comput. Struct.*, **45**(5), 841-874.
Barton, M.V. (1951), "Vibration of rectangular and skew cantilever plates", *ASME J. Appl. Mech.*, **18**, 129-134.
Coté, A. and Charron, F. (2001), "On the selection of *p*-version shape functions for plate vibration problems", *Compu. Struct.*, **79**, 119-130.
Dokainish, M.A. and Rawtani, S. (1971), "Vibration analysis of rotating cantilever plates", *Int. J. Num. Meth. Eng.*, **3**, 233-248.
Gordon, W.J. and Hall, C.A. (1973), "Transfinite element methods: Blending-function interpolation over arbitrary curved element domains", *Numer. Mathe*, **21**, 109-129.
Hamza-cherif, S.M. and Houmat, A. (2004), "Natural frequencies of rotating flexible beams by using hierarchical finite element method", *Proc. of 8th Pan. Amer. Cong. of Appl. Mech.*, Havana, **10**, 101-104.
Houmat, A. (1997), "An alternative hierarchical finite element method formulation applied to plate vibrations", *J. Sound Vib.*, **206**(2), 201-215.
Houmat, A. (2001), "A sector Fourier *p*-element applied to free vibration analysis of sector plates", *J. Sound Vib.*, **243**(2), 269-282.
Kane, T., Ryan, R. and Banerjee, A. (1987), "Dynamics of a cantilever beam attached to a moving base", *J. of Guidance, Control and Dynamics*, **10**, 139-151.
Langley, R.S. and Bardell, N.S. (1998), "A review of current analysis capabilities applicable to the high frequency vibration prediction of aerospace structures", *The Aeronautical Journal*, **102**, 287-297.
Leissa, A. (1974), "On a curve veering", *J. of Applied Mathematics and Physics*, **25**, 99-111.
Meirovitch, L. and Baruh, H. (1983), "On the inclusion principle for the hierarchical finite element method", *Int. J. Num. Meth. Eng.*, **19**, 281-291.
Putter, S. and Manor, H. (1967), "Natural frequencies of radial rotating beams", *J. Sound Vib.*, **56**, 175-185.
Ramamurti, V. and Kielb, R. (1984), "Natural frequencies of twisted rotating plates", *J. Sound Vib.*, **97**(3), 429-449.
Southwell and Gough (1921), "The free transverse vibration of airscrew blades", British *A.R.C., Report and Memoranda*, 655.
Szabo, B.A. and Sahrmann, G.J. (1988), "Hierarchical plate and shells models based on *p*-extension", *Int. J. Num. Meth. Eng.*, **26**, 1855-1881.
Szabo, B.A. and Babuška, I. (1991), *Finite Element Analysis*, John Wiley & Sons. Inc., New York.
Yoo, H., Ryan, R. and Scott, R. (1995), "Dynamics of flexible beams undergoing overall motions", *J. Sound Vib.*, **10**, 139-148.
Yoo, H. and Chung, J. (2001), "Dynamics of rectangular plates undergoing prescribed overall motions", *J. Sound Vib.*, **239**, 123-137.
Yoo, H. and Pierre, C. (2003), "Modal characteristic of a rotating rectangular cantilever plate", *J. Sound Vib.*, **259**(1), 81-96.
Zhu, D.C. (1986), "Development of hierarchical finite element method at BIAA", *Proc. of the Int. Conf. on Computational Mechanics,* Tokyo, **I**, 123-128.

Notation

a, b	: plate element length in the x direction and y direction
b^i, b^{i+1}	: plate element length of adjacent elements
$[A(\theta)]$	: orthogonal rotation matrix
h	: plate thickness
$D = Eh^3/12(1-\nu^2)$	: flexural rigidity
E	: Young's modulus
$f(\eta)$, $g(\eta)$	: shape functions for stretching and bending respectively

G : shear modulus
$G_{m,n}$: elements of the gyroscopic matrix
$M_{m,n}$, $K_{m,n}$: elements of the mass and stiffness matrix respectively
M_w, N_w : number of the trigonometric shape functions in X and Y direction
$[N]$: matrix of the shape functions
$\{q\}$: vector of generalized co-ordinates
r_p, R_p : local and global position respectively
$R_{m,n}$: elements of the additional centrifugal stiffness matrix
R_h : hub radius
S, R : arc-length stretch non-Cartesian displacements
T, U : kinetic and strain energy of the rotating plate
U_i, U_b : in-plane and bending strain energy of the plate
(u, v, w) : displacements in X, Y, Z co-ordinates
$\overline{X}$, $\overline{Y}$, $\overline{Z}$: global co-ordinates
X, Y, Z : local co-ordinates
X_{kl}, Y_{kl}, Z_{kl} : elements of the vector of generalized co-ordinates
θ : plate rigid body rotation
$\mu = a^2(\rho h/D)^{0.5}\Omega$: angular speed parameter
ν : Poisson's ratio
ρ : mass per unit area
ω : bending frequency (rd/s)
$\omega^* = a^2(\rho h/D)^{0.5}\omega$: frequency parameter
Ω : angular speed of the plate (rd/s)
$\dot{\Omega}$: angular acceleration of the plate
ξ, η : non-dimensional co-ordinates
α, β : order of derivative of the shape functions